Results from a Synthetic Model of the ITER XRCS-Core Diagnostic Based on High-Fidelity X-Ray Ray Tracing

N.A. Pablant,[1, a)] Z. Cheng,[2] M. O'Mullane,[3] L. Gao,[1] R. Barnsley,[2] M.N. Bartlett,[4] M. Bitter,[1] E. Bourcart,[5] G.V. Brown,[6] M. De Bock,[2] L.F. Delgado-Aparicio,[1] C. Dunn,[7] A.J. Fairchild,[6] N. Hell,[6] K.W. Hill,[1] J. Klabacha,[1] F. Kraus,[1] D. Lu,[8] P.B. Magesh,[9] S. Mishra,[9] M. Sánchez del Río,[10] R. Tieulent,[2] and Y. Yakusevich[11]

[1)] *Princeton Plasma Physics Laboratory, 100 Stellarator Road, Princeton, New Jersey 08543, USA*
[2)] *ITER Organization, Route de Vinon-sur-Verdon, CS 90 046, 13067 St. Paul Lez Durance Cedex, France*
[3)] *University of Strathclyde, 107 Rottenrow, Glasgow G4 0NG, UK*
[4)] *University of Illinois at Urbana-Champaign, 104 S. Wright Street Urbana, IL 61801, USA*
[5)] *Carnegie Mellon University, 5000 Forbes Ave, Pittsburgh, PA 15213, USA*
[6)] *Lawrence Livermore National Laboratory, 7000 East Ave., Livermore, CA 94550, USA*
[7)] *Plasma Science Fusion Center, MIT, Cambridge, Massachusetts 02139, USA*
[8)] *Institute Of Plasma Physics, No. 350 shushanhu Road, Hefei, Anhui, CHINA*
[9)] *ITER-India, Institute for Plasma Research, Koteshwar, Gandhinagar, 382 424, Gujarat, INDIA*
[10)] *European Synchrotron Radiation Facility, B.P. 220, 38043, Grenoble Cedex, FRANCE*
[11)] *University of California San Diego, 9500 Gilman Dr., La Jolla, CA 92093, USA*

(Dated: 25 June 2024)

A high-fidelity synthetic diagnostic has been developed for the ITER Core X-Ray Crystal Spectrometer diagnostic (XRCS-Core) based on x-ray ray tracing. This synthetic diagnostic has been used to model expected performance of the diagnostic, to aid in diagnostic design, and to develop engineering tolerances. The synthetic model is based on x-ray ray tracing using the recently developed `XICSRT` ray tracing code and includes fully three-dimensional representation of the diagnostic based on the computer aided design (CAD). The modeled components are: plasma geometry and emission profiles, highly oriented pyrolytic graphite (HOPG) pre-reflectors, spherically bent crystals, and pixelated x-ray detectors. Plasma emission profiles have been calculated for Xe^{44+}, Xe^{47+} and Xe^{51+}, based on an ITER operational scenario available though the Integrated Modelling & Analysis Suite (IMAS) database, and modeled within the ray tracing code as a volumetric x-ray source; the shape of the plasma source is determined by equilibrium geometry and an utilizes an appropriate wavelength distribution to match the expected ion temperature profile. All individual components of the x-ray optical system have been modeled with high-fidelity producing a synthetic detector image that is expected to closely match what will be seen in the final as-built system. Particular care is taken to maintain preservation of photon statistics throughout the ray tracing allowing for quantitative estimates of diagnostic performance.

Keywords: ray tracing, x-ray spectroscopy, ITER

I. INTRODUCTION

The X-Ray Crystal Spectrometer, Core Viewing (XRCS-Core) is a key diagnostic for the ITER tokamak to measure ion temperature and plasma flow, amongst other measurements[1]. Because this diagnostic is intended for use in a burning plasma environment, it features a novel design that combines x-ray pre-reflectors with a traditional high-resolution spherical-crystal design to achieve three objectives: 1) a wide range of viewing angles in the plasma, 2) small wall penetration and minimization of neutron streaming, 3) placement of the detector far from the plasma in a neutron shielded location.

The novel aspects of this spectrometer have motivated the development of a synthetic diagnostic model based on x-ray ray tracing to aid in design, evaluate the expected performance, and verify fast synthetic models. The ray tracing simulation presented here includes detailed models of the 3D plasma emission and each of the x-ray optical components, and aims to produce high-fidelity synthetic images that closely match the expected output of the actual physical system.

II. ITER XRCS-CORE DIAGNOSTIC DESCRIPTION

The XRCS-Core diagnostic is an integrated set of x-ray spectrometers that utilize Doppler spectroscopy techniques to measure time resolved profiles of several different important parameters: ion temperature, plasma flow, electron temperature, and impurity charge state densities. The impurity charge state densities can be used to constrain the radiated power. The measurements rely on the emission from highly ionized impurities that are either deliberately injected into the plasma for diagnostic purposes (xenon) or which are present intrinsically (tungsten). To cover the very wide range of temperatures found across the plasma, lines from several different charge states are used: Xe^{44+} (2.5525 Å), Xe^{47+} (2.5575 Å), Xe^{51+} (2.1899 Å) and W^{64+} (1.3589 Å).

[a)] Electronic mail: npablant@pppl.gov

Emission line wavelengths for Xe^{44+} and Xe^{47+} were taken from measurements made at LLNL's EBIT-I electron beam ion trap as part of the diagnostic design[2]. Details of these Xe line emission measurements will be provided in a forthcoming publication.

A novel design is used for XRCS-Core in which a set of 11 planar pre-reflectors, placed near the diagnostic first wall (DFW), are used to direct x-ray photons back to a set of 6 spherically bent Bragg crystals (which will be referred to as 'resolving crystals') which in turn disperse the x-ray emission onto a set of 2 detectors. Each resolving crystal utilizes different lattice planes of germanium: 3 × Ge (1 1 3) for Xe^{44+} & Xe^{47+} (*red*, *magenta*, *lime*), 2 × Ge (0 0 4) for Xe^{51+} (*blue*, *yellow*), and 1 × Ge (3 3 5) for W^{64+} (*green*), where the colors refer to the cyrstal labels and correspond to coloring in subsequent figures and tables. Each pre-reflector captures light from a different volume in the plasma, and therefore defines a sightline in the system. The system also includes 6 straight-through sightlines, one for each resolving crystal, making for a total of 17 sightlines. The configuration of the sightlines, location of the pre-reflectors, and the five xenon viewing crystals can be seen in Fig.1.

The pre-reflectors are made of highly oriented pyrolytic graphite (HOPG) with a mosaicity of around 0.4° and utilize the (0 0 2) reflection plane. The mosaicity of the HOPG provides the pre-reflectors with a very broad effective Bragg reflection acceptance angle which enables a sufficiently broad bandwidth in this two-crystal Bragg reflection scheme and reduces requirements on alignment between the pre-reflector and the resolving crystals. The resolving crystals, along with the distance between the crystals and the detectors, completely define the energy resolution of the system. In this way, each of the crystal-detector combinations acts as a traditional X-Ray Imaging Crystal Spectrometer (XICS)[3] in which the 1D imaging property is being used in conjunction with the pre-reflectors to define a set of discrete sightlines into the ITER plasma.

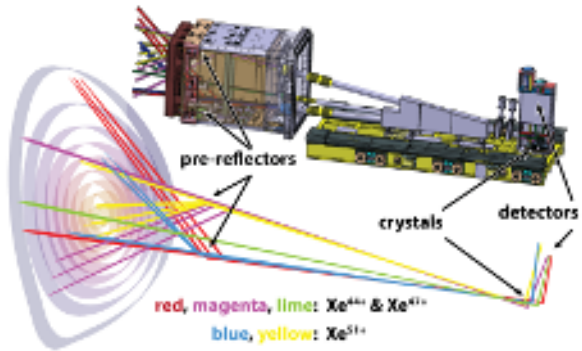

FIG. 1. CAD model (top) and ray tracing model (bottom) of the XICS-Core diagnostic. Ray tracing shows only the rays that originate in the plasma and intersect with the detector. The total length of the diagnostic shown in this figure is approximately 9 m.

Additional details of the XRCS-Core design can be found in Ref. 1, which represents a previous design configuration from the conclusion of the Conceptual Design Review (CDR); The results in this paper focus on a new design, which matches the configuration at the Preliminary Design Review (PDR) held in October of 2023 and consists of the following changes: **a)** The system now uses the Xe^{44+} line at 2.5525 Å instead of the one at 2.7203 Å; This enables the nearby Xe^{47+} line to be measured simultaneously. **b)** An additional Ge (1 1 3) crystal has been added on the same substrate as the W^{64+} Ge (3 3 5) crystal providing a central straight-through sightline for Xe^{44+}/Xe^{47+}. **c)** The orientation of the pre-reflectors have been changed to provide sightlines that are optimized for better coverage in lower temperature plasmas.

III. THE XICSRT RAY TRACING CODE

To enable the development of a synthetic diagnostic for the ITER XRCS-Core diagnostic, a new general purpose x-ray ray tracing code has been developed, named `XICSRT`[4,5]. This code, `XICSRT`, has been designed with a focus on simplicity, extensibility, and preservation of photon statistics; it is implemented in pure python with a generalized 3D coordinate system that simplifies modeling of plasma emission and specification of x-ray optical components taken from either analytical calculations or CAD design. This ray tracing code, while originally developed for ITER XRCS-Core, has also now been applied to synthetic diagnostic modeling on the Wendelstein 7-X (W7-X) stellarator[6,7], the National Ignition Facility (NIF)[4,8] and the OMEGA laser facility[9]. The `XICSRT` code has been verified against several other ray tracing codes including `SHADOW`[10], `XRSA`[1], `ToFu`[11], and `LUX/BMAD`[12]. The following is a description of the modeled components in the `XICSRT`.

The X-Ray emission source is modeled using a 3D description of the ITER plasma equilibrium shape and flux surfaces as defined through the Integrated Modelling & Analysis Suite (IMAS) database for the given simulation "shot". For the present work the Xe line emissivity and temperature are assumed to be constant on a flux surface and defined by a 1D radial profile while the plasma flow velocity is set to zero. To model the emission within the full 3D plasma volume a randomized set of ray bundles are created. Within each ray bundle a set of rays is created based on a Monte-Carlo approach with the number of rays based on the emissivity of the plasma at the given location (using randomized Poisson statistics) and a wavelength distribution based on the temperature and plasma flow (using a Voigt distribution for Doppler width and natural line broadening and with each ray given a Doppler shift for the given ray direction). The generated rays are produced in a small volume around the bundle center. To improve ray tracing efficiency, rays from each bundle are emitted in an isotropic cone aimed at the first optical element with an angular spread sufficient to over-

fill the element.

The first x-ray optic in the ray tracing chain is the HOPG pre-reflector. To model reflections from HOPG, a micro-model has been developed within XICSRT to mimic the mosaic reflection process. For each ray intersecting the surface the incident angle is compared with a normal vector based on the surface normal plus a randomized angular orientation that represents the mosaic crystalites that make up the HOPG bulk, with a distribution based on the "mosaicity" of the reflector. The incoming ray (photon) is then either probabilistically reflected based on Bragg reflection within the diffraction profile (rocking curve) of a pure graphite crystal, or assumed to penetrate to the next encountered crystalite. This process of randomizing the surface normal based on the mosaic distribution and checking for Bragg reflection is repeated up to a number of times that represents the penetration depth for a given x-ray energy. The number of mosaic iterations is informed by secondary extinction depth calculations[13] and ultimately chosen to match the analytic peak reflectivity calculated by XOP[14–16]. Comparisons between the mosaic micro-model in XICSRT and the macro-model implemented in XOP and SHADOW[10] show good agreement in terms of both the effective rocking curve shape and in capturing the "parafocusing" effect, and give confidence to this approach. In the current simulation work the HOPG crystal modeled using the (0 0 2) reflection plane, a mosaicity of 0.4°, a depth of 22 iterations, a crystal d-spacing of 3.3480 Å and graphite crystal rocking curve width of 77 µrad (FWHM).

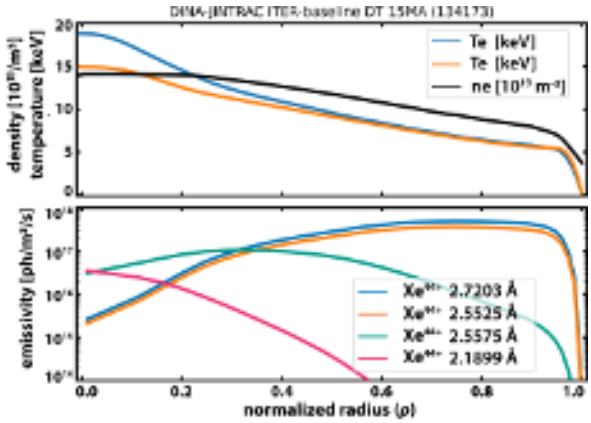

FIG. 2. Modeled plasma profiles and Xe line emissivity for an ITER DT 15 MA baseline scenario.

The next x-ray optic is the spherical resolving crystal. This resolving crystal is modeled as a spherical reflector with a probabilistic model for ray reflection based on the perfect crystal diffraction profile[17], and checked against XOP for bent crystal broadening. For the current work the incoming x-ray light is considered to be unpolarized and only the *s*-polarization rocking curve is considered.

Finally, rays that reflect from both the HOPG pre-reflector and the resolving crystal are recorded at the detector. Each of the two detectors in the diagnostic design, and modeled in the synthetic diagnostic, are a photon counting Dectris Pilatus 3 pixelated hybrid-CMOS detectors with pixel-pitch of 172 µm and made up of five stacked modules of 487 × 195 pixels.

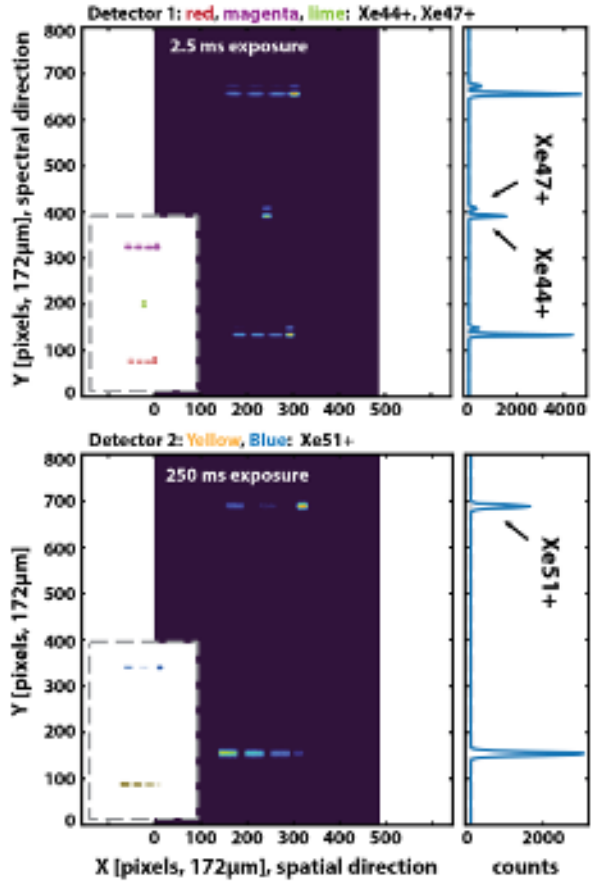

FIG. 3. Synthetic diagnostic images on each of the two simulated Pilatus 3 detectors. The inlaid images show ray intersections with the detector plain. The plot on the right of each image show a histogram of intensity vs. pixel in the wavelength direction with counts summed along the horizontal (spatial) direction.

IV. SYNTHETIC DIAGNOSTIC RESULTS

For the synthetic diagnostic modeling described herein, we have chosen to focus on an ITER baseline D-T scenario with 15 MA of plasma current. We have used plasma profiles as modeled using the JINTRAC-DINA analysis code chain and described in Ref. 18,19 (IMAS 134173 r106). Modeling of the charge state density and Xe line emission was completed using SANCO coupled with ADAS and included a simple model for impurity transport[20]; details on the line emission modeling will be reported in a forthcoming publication. For these simulations the total Xe concentration has been set relative

to the electron density to be $n_{Xe}/n_e = 1 \times 10^{-5}$ (a volume integrated normalization was used). The modeled plasma profiles and line emissivities are shown in Fig.2.

The final simulated images on each of the two modeled detectors are shown in Fig.3. These images show that the emission of each sightline is well focused and separated in the horizontal (spatial direction). In addition, the Xe^{44+} and Xe^{47+} lines are clearly separated even with the substantial Doppler broadening in this high-temperature plasma scenario. The x-ray ray tracing in `XICSRT` is photon statistics preserving throughout the entire simulation, and so both the absolute intensity on the detector and the Poisson distributed photon noise are predictive for this plasma scenario. With this in mind, it is possible to predict the brightness of each sightline in terms of photons/second, as shown in Table I.

As the primary purpose of this set of simulations was to look at line brightness and spectral separation, the current simulations do not include background Bremsstrahlung emission from the plasma or background neutrons and associated gamma rays that impact the detector. These sources can be easily included, and will be an important part of future integrated simulation work.

Xe44+ sightlines	Photons/second	Time Resolution
red_1	1.5×10^6 (±0.03)	6 ms
red_2	1.9×10^6 (±0.03)	5 ms
red_3	1.9×10^6 (±0.03)	5 ms
red_s	3.6×10^6 (±0.04)	3 ms
magenta_1	2.4×10^6 (±0.03)	4 ms
magenta_2	1.9×10^6 (±0.03)	5 ms
magenta_3	1.8×10^6 (±0.03)	6 ms
magenta_s	5.5×10^6 (±0.05)	2 ms
lime_s	3.5×10^6 (±0.04)	3 ms
Xe47+ sightlines	**Photons/second**	**Time Resolution**
red_1	1.8×10^4 (±0.3)	543 ms
red_2	3.8×10^4 (±0.4)	260 ms
red_3	8.4×10^4 (±0.6)	119 ms
red_s	8.0×10^5 (±0.2)	12 ms
magenta_1	1.7×10^5 (±0.1)	58 ms
magenta_2	2.9×10^5 (±0.1)	34 ms
magenta_3	3.7×10^5 (±0.1)	27 ms
magenta_s	5.9×10^5 (±0.2)	17 ms
lime_s	8.6×10^5 (±0.2)	12 ms
Xe51+ sightlines	**Photons/second**	**Time Resolution**
blue_1	2.4×10^3 (±0.1)	4112 ms
blue_2	1.1×10^4 (±0.02)	912 ms
blue_s	4.3×10^4 (±0.04)	235 ms
yellow_1	1.8×10^4 (±0.02)	542 ms
yellow_2	3.9×10^4 (±0.04)	257 ms
yellow_3	6.3×10^4 (±0.05)	159 ms
yellow_s	3.3×10^3 (±0.1)	2990 ms

TABLE I. Expected total photons-per-second of each sightline of the XRCS-Core system. The error range comes from the limited number of rays at the detector in the raytracing simulations (Poisson statistics). The time resolution represents the time to accumulate 10,000 photons, which corresponds to a relative error in the measured line brightness of 1%.

As described in Section III, the addition of a pre-reflector does not affect the dispersion or energy resolution of the x-ray spectrometer system; however, this two-crystal scheme does affect the bandwidth of the system. To study the wavelength/energy bandwidth of the XRCS-Core diagnostic a simplified ray tracing model is utilized in which the ITER plasma is replaced by a planar area x-ray source with uniform wavelength emission. The results of this simulation, for representative sightlines, can be seen in Fig.4. The most notable feature in this study is the difference between the bandwidth curves between the 'red' and 'magenta' crystals versus the 'blue' and 'yellow' crystals. This difference is explained by the relative direction of reflection between the pre-reflector and the resolving crystal; In one case the crystal and pre-reflector face the same way and the dispersion direction for long and short wavelengths is matched and in the other case the orientation (and dispersion direction) are opposite[21].

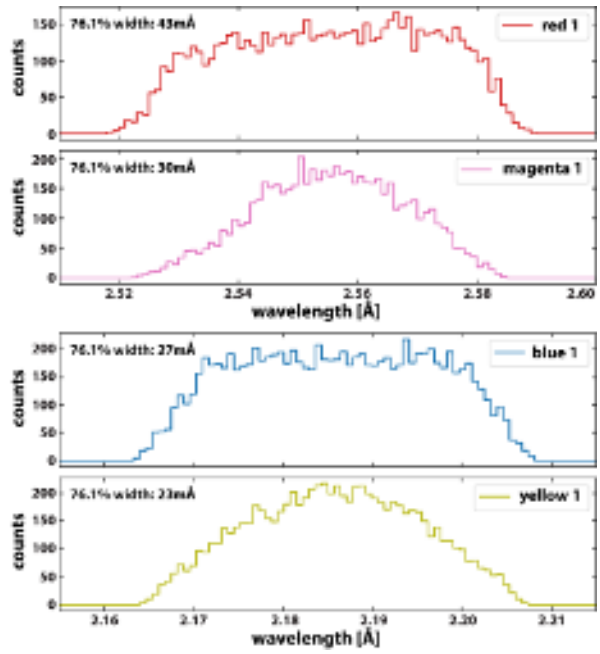

FIG. 4. Wavelength bandwidth for representative sight-lines from each of the four Xe spectrometer channels. Each subplot shows a histogram of counts on the detector given a source with a uniform wavelength distribution.

With a dual reflector design, a critical consideration is the required alignment between the pre-reflectors and the resolving crystal. The `XICSRT` synthetic diagnostic has been used to explore alignment tolerances. This exploration of varying the relative position and angle between the two crystals in ray tracing has led to several conclusions: the angular alignment is highly sensitive in only one direction, along the direction of Bragg reflection; in this direction a relative crystal alignment of 0.1° is required to maintain a peak throughput in the bandwidth within about 10%. Due to the wide effective diffraction profile of the HOPG, the system is otherwise relatively insensitive to angular or transnational displacements in

comparison to achievable engineering tolerances. This result has been a driving factor in the engineering of the ITER port-plug and the mounting and cooling solutions for the pre-reflectors. The expected thermal displacement of the pre-reflectors in the preliminary design has been captured from ANSYS analysis and modeled in `XICSRT`, and indicates that the bandwidth distortion is acceptable.

V. CONCLUSIONS

Synthetic diagnostic modeling, enabled by high-fidelity x-ray ray tracing, has provided performance predictions for the ITER XRCS-Core diagnostic. This modeling has shown good focusing and energy resolution for all Xe channels including all 11 pre-reflected and 5 straight sightlines. These simulations, performed with careful attention to photon throughput and photon statistics, have enabled quantitative predictions of line brightness on the detector and an estimation of achievable temporal resolution.

The XRCS-Core was designed to provide temperature profile measurements over a wide range of plasma conditions and central plasma temperatures. Different ITER plasma simulation models produce a variety of expected profiles, and the JINTRAC-DINA result recommended by the ITER team and used in this work is notable in that it predicts a central electron and ion temperature significantly below that of other modeling efforts for the full curent DT scenario[22]. In the case that the ITER plasma achieves a higher plasma temperature than used in this modeling, the Xe^{51+} emission will play a more important diagnostic role in the inner portion of the plasma with brighter lines (and shorter estimated integration times) for the relevant sightlines.

Importantly, the simulations performed with `XICSRT` closely match and verify the fast analytical/ray tracing mixed code `XRSA`[1] which was used for iterative design of the XRCS-Core diagnostic. In the future, the `XICSRT` synthetic diagnostic model, along with its refinements, will be a critical part of the development of an analysis tool chain for the ITER XRCS-Core diagnostic including development of discrete sightline tomographic inversion techniques.

ACKNOWLEDGMENTS

This work was performed under the auspices of the U.S. Department of Energy by Princeton University under contract number DE-AC02-09CH11466, Lawrence Livermore National Laboratory under Contract DE-AC52-07NA27344 and is supported by funding from US-ITER. The views and opinions expressed herein do not necessarily reflect those of the ITER Organization.

AUTHOR DECLARATIONS

Conflict of Interest

The authors have no conflicts to disclose.

DATA AVAILABILITY

The data that support the findings of this study are openly available at `https://datacommons.princeton.edu`.

REFERENCES

[1] Cheng, Z., Bader, A., De Bock, M. et al. Review of Scientific Instruments, **93**, 7, 073502 (2022). https://doi.org/10.1063/5.0080718.
[2] Brown, G.V., Hell, N. and Fairchild, A. in preparation (2024).
[3] Bitter, M., Hill, K., Gates, D. et al. Review of Scientific Instruments, **81**, 10, 10E328 (2010).
[4] Pablant, N.A., Bitter, M., Efthimion, P.C. et al. Review of Scientific Instruments, **92**, 9, 093904 (2021). https://doi.org/10.1063/5.0054329.
[5] *XICSRT sourcecode* (2021). https://github.com/PrincetonUniversity/xicsrt.
[6] Pablant, N.A., Langenberg, A., Alonso, J.A. et al. Review of Scientific Instruments, **92**, 4, 043530 (2021). https://doi.org/10.1063/5.0043513.
[7] Kring, J., Pablant, N., Langenberg, A. et al. Review of Scientific Instruments, **89**, 10F107 (2018).
[8] Pablant, N.A., Bitter, M., Gao, L. et al. Review of Scientific Instruments, **93**, 10 (2022). 103548, https://doi.org/10.1063/5.0101856.
[9] Cordova, T., MacDonald, M.J., Döppner, T. et al. Review of Scientific Instruments, **93**, 8, 083509 (2022). https://doi.org/10.1063/5.0099176.
[10] Sanchez del Rio, M., Canestrari, N., Jiang, F. and Cerrina, F. Journal of Synchrotron Radiation, **18**, 5, 708 (2011).
[11] Da Ros, A., Vezinet, D., Colledani, G. et al. Review of Scientific Instruments, **95**, 4, 043505 (2024). https://doi.org/10.1063/5.0179905.
[12] Sagan, D. Nuclear Instruments and Methods in Physics Research Section A, **558**, 1, 356 (2006).
[13] Zachariasen, W.H. *Theory of X-ray Diffraction in Crystals*. Dover Publications (1967).
[14] del Río, M.S. and Dejus, R.J. Proc SPIE, **8141**, 368 (2011).
[15] Sánchez del Río, M., Bernstorff, S., Savoia, A. and Cerrina, F. Review of Scientific Instruments, **63**, 1, 932 (1992). https://doi.org/10.1063/1.1143784.
[16] Sanchez Del-Rio, M. *Mosaic crystals in shadow: an update*. Tech. rep. (2013). https://github.com/srio/shadow3-docs/blob/master/doc/report-shadow-mosaics.pdf.
[17] *X0h: X-ray dynamical diffraction data on the Web* (2021). Https://x-server.gmca.aps.anl.gov/x0h.html.
[18] Koechl, F., Pinches, S., Casson, F. et al. In *Proceedings of the International Atomic Energy Agency Fusion Energy Conference (IAEA-FEC)*, EX/P7–25 (2018).
[19] Koechl, F., Ambrosino, R., Belo, P. et al. Nuclear Fusion, **60**, 6, 066015 (2020).
[20] O'Mullane, M., Cheng, Z. and Pablant, N. (2024). In preparation.
[21] Gao, L., Pablant, N., Cheng, Z. et al. Review of Scientific Instruments (2024). In preparation.
[22] Garzotti, L., Belo, P., Corrigan, G. et al. Nuclear Fusion, **59**, 2, 026006 (2018).